

Analysis of the Photothermal Engine Cycle in an AFM-IR Measurement of Photothermal Expansion

Luca Quaroni

Department of Physical Chemistry and Electrochemistry, Faculty of Chemistry, Jagiellonian University, 30-387, Kraków, Poland

e-mail: luca.quaroni@uj.edu.pl

Keywords: Photothermal effect; AFM-IR; micro engine; infrared spectroscopy

Abstract

The thermomechanical processes that underlie AFM-IR measurements of the photothermal effect are collectively described in terms of a thermodynamic engine cycle. We use it to derive practical guidelines for performance optimization in AFM-IR experiments.

Introduction

Measurement of the photothermal effect allows spectroscopic and imaging experiments covering a wide spectral range. Among the multiple measurement configurations, the use of atomic force microscopy (AFM) instrumentation to detect photothermal expansion is receiving increasing attention. Interest is driven by the promise of spectroscopic analysis in the mid-infrared (mid-IR) spectral region ($\lambda \sim 2.5 - 25 \mu\text{m}$) with nanoscopic resolution, much better than allowed by the optical diffraction limit.¹ Delivery on such promise would extend the impact of IR absorption spectroscopy to nanoscale samples, a development of great interest to both academic and industrial researchers. The deflection of an AFM cantilever following photothermal expansion with mid-IR was first demonstrated by Anderson using conventional benchtop instrumentation for Fourier-Transform Infrared (FTIR) spectroscopy.² The method was later developed into a technique for spectroscopic analysis by Alexandre Dazzi's group using a Free-Electron laser as a light source.³ The implementation with benchtop laser sources has further widened its appeal and its accessibility to a larger pool of researchers and opened the way to its commercialization, making it a rapidly growing technique of wide appeal to diverse research disciplines. Different names are currently used to describe the various incarnations of photothermal measurements with AFM detection, including AFM-IR and Photothermal Induced Resonance (PTIR). In the present work, the term AFM-IR will be the main moniker.

Despite increasing popularity, several fundamental aspects of the technique are unclear, and many experimental observations are still unexplained by existing theoretical models. The difficulty arises from the complexity of the specific signal transduction mechanism, which involves a micro mechanical scheme to detect light-induced heating in a nanoscopic location.

The possibility to relate the absorption spectrum from an AFM-IR measurement to its far-field equivalent, relies on having a detailed understanding of the physical processes involved in signal generation and how they relate to the absorption coefficient. It is already appreciated

that the scanning probe detection mechanism introduces a dependence of the signal from the mechanical properties of tip-sample interaction.⁴

A less studied aspect is the role of heat-transfer processes on signal generation. This facet has been addressed using Fourier's heat transfer theory⁴, however a thermodynamic treatment is still missing. It is the purpose of this work to take the first steps to address this shortcoming. The approach is based on the consideration that, in thermodynamic terms, the AFM-IR experiment is based on a microscopic engine, a device that converts energy into work. In an AFM-IR measurement, radiation energy is converted into the work necessary to deflect the cantilever of the AFM probe. In the following sections we will assess the viability of an engine thermodynamic cycle to describe the performance of AFM-IR measurements.

Results and Discussion

The basic AFM-IR experiment as a photothermal engine.

A graphical representation of the basic AFM-IR experiment is shown in Figure 1, panel A. AFM-IR measures light absorption via the expansion of the absorbing region induced by the photothermal effect. The sample is mounted as for a conventional AFM experiment. Irradiation occurs by focusing light at the tip-sample contact region. An absorbing sample expands upon illumination and the expansion is recorded via the deflection of the cantilever of the AFM probe and quantified by the movement of the AFM monitor laser on a four-quadrant detector. The deflection is generally assumed to be proportional to the local absorption coefficient of the sample at the wavelength of irradiation and is used for spectroscopic analysis, although this proposition has never been confirmed by matching theoretical and experimental results. AFM-IR measurements can be carried in both a spectromicroscopy and an imaging configuration. In the former, the probe is kept stationary while the light source is scanned through the spectral range of interest. In the imaging configuration the AFM tip is scanned over the sample while the light source is pulsed in synchrony at a single wavelength.

A thermodynamic analysis of the AFM-IR experiment relies on the definition of a cycle that best describes the processes occurring during turnover. The first step in the analysis is the ideal breakdown of the measurement into the separate steps of a cyclic process. The most obvious possibility is shown in Figure 1, panel B. The sample is in an initial state (State 1) described by a set of thermodynamic variables. We choose the pressure (P), volume (V) and temperature (T) set. Light absorption delivers energy to the sample, simultaneously increasing both T and P (State 2). The increase in T and P leads to sample expansion (State 3). In the transition from State 2 to State 3, the expansion acts against the force exerted by the cantilever and causes its deflection. The expanded sample cools back down to the initial temperature (typically room temperature) leading to State 4. In the last step the cooled (thermalized) sample, described by a lower pressure than is exerted by the AFM tip, is compressed back to its initial volume, corresponding to the initial state.

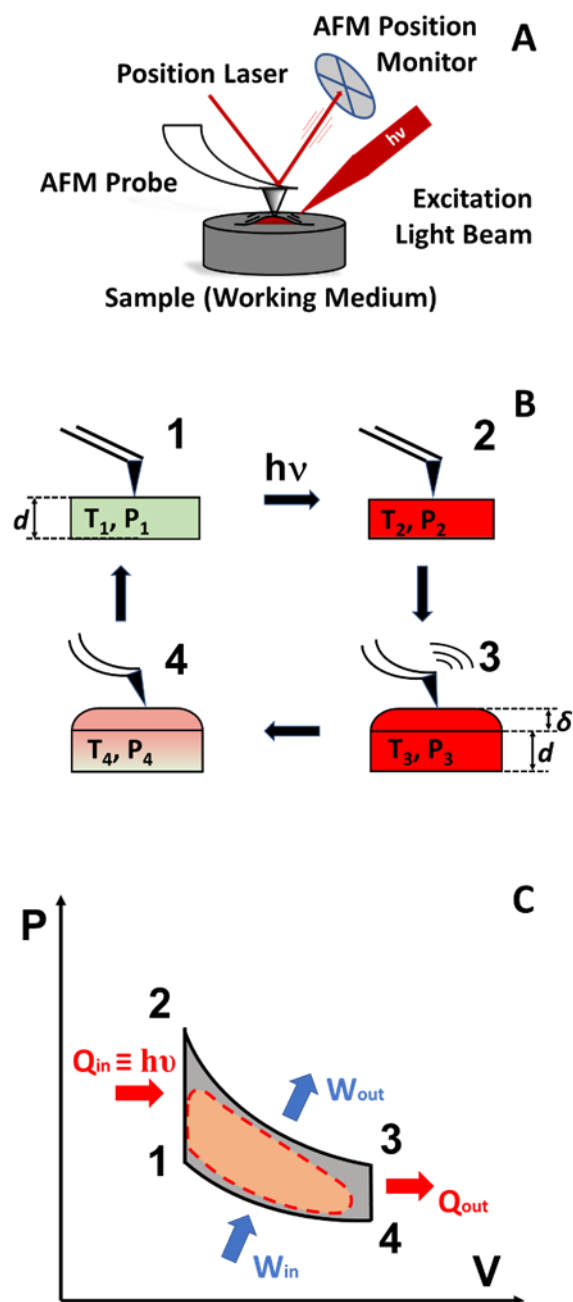


Figure 1. AFM-IR signal generation as an engine cycle. **A.** The AFM-IR experiment. **B.** States of the engine and transformations. T_n, P_n, V_n : respectively, temperature, pressure and volume of state n . d sample thickness. δ Sample expansion/cantilever deflection. **1.** Resting state. **2.** After heating following from light absorption. **3.** After isothermal expansion of state **2**. **4.** After isochoric thermalization of state **3**. Red color graphically indicates higher temperature. **B.** The AFM-IR engine cycle. Numbering of cycle points matches the states of Figure 1A.

It is valuable to represent such cycle in a PV diagram, as for conventional macroscopic engines (Black lines in Figure 1, panel C). The working medium of the engine is the light absorbing material. The transition from State 1 to State 2 represents absorption of photons to generate an excited energy state, corresponding to increased internal energy and increased temperature,

from T_1 to T_2 . Photon absorption and the corresponding temperature increase are described by a single isochorous transformation, between State 1 and State 2, a vertical line in the PV diagram. The transformation between State 2 and State 3 is an expansion that progresses until the internal pressure of the sample balances the recall force of the cantilever. The expansion is assumed rapid compared to thermal exchange between sample and environment, corresponding to an isothermal transformation at the temperature $T_2 (=T_3)$. This is represented by a hyperbole in the PV plane. The thermalization of the expanded sample occurs by heat exchange with the surrounding environment and is also assumed to be a rapid isochorous transformation, bringing the system from State 3 to State 4. The final compression step, which regenerates the initial State 1 from State 3 is assumed to be a second isothermal process at the initial temperature T_1 . Overall, energy is absorbed by the engine in the form of photons during transformation 1 - 2 and is released as heat during transformation 3 - 4. Work is performed by the expanding medium on the cantilever during transformation 2 - 3 and is performed by the cantilever on the working medium during transformation 4 - 1.

The cycle of Figure 1C is analogous to the working cycle of a classical Stirling engine operating between two thermal reservoirs at T_1 and T_2 . The similarity is reinforced by the retention of the working medium, which is not exchanged with the environment, throughout multiple cycles. The use of a radiation source as the external energy source, in place of heat, qualifies it as a microscopic Stirling solar engine. In analogy with mechanical engines, the AFM probe acts as the piston. The cantilever of the probe is deflected by the expansion and contraction of the sample and the tip maintains contact with the sample throughout the cycle. The cantilever and tip act as a spring-loaded piston and respond to expansion and contraction of the working medium with a harmonic force. In this respect it is also the equivalent of a piston and displacer pair in some designs of free piston Stirling engines.

The cycle marked by solid black lines in Figure 1C is to be considered as an ideal cycle, in which each of the four steps is performed as an individual, infinitely slow quasi-static transformation. In a real situation the cycle develops over a finite time and the four processes cannot be fully separated. Among the assumptions implied in the construction of the ideal cycle, the more realistic one is the isochoric nature of transformation 1 - 2, justified by the time scale of the optical absorption process and following relaxation. In the most general case of a real engine, thermalization of the sample is ongoing throughout transformations 2 - 3, 3 - 4, and 4 - 1, and the resulting real PV cycle is closer to the one represented by the dotted red line of Figure 1C.

The thermodynamic description of Figure 1 allows extracting useful relationships between the thermomechanical properties of the engine and its performance, both in generating the AFM-IR signal and as a micro-optomechanical engine in general. A quantitative description of the system can provide further insight and will be the subject of this and the following sections.

The systems probed by AFM-IR experiments extend from the macroscopic scale, described by classical thermodynamics, to the molecular scale and different theoretical approaches are required to model them. The present analysis will address the workings of macroscale to nanoscale regimes.

The non-ideal photothermal engine.

The analysis of the cycle of Figure 1 lays on the ideal assumption of quasi-static operation. For finite evolution times, expansion and contraction of the working medium are far from ideal, since cooling of the sample occurs rapidly and continuously during both stages. Heat dissipation takes place at multiple interfaces, including the sample-substrate, sample-tip, and sample-air interfaces, plus any interfaces between sample phases.

The effect of the resulting real PV cycle on performance parameters is graphically represented in Figure 2. Faster heat dissipation under non-thermostatic conditions leads to a smaller area of the cycle. In turn this corresponds to decreased W_{tot} , reduced expansion ($V''_{max} < V'_{max} < V_{max}$) and deflection ($\delta''_{max} < \delta'_{max} < \delta_{max}$), and a weaker AFM-IR signal.

It is desirable to design the engine cycle to correct for these factors. Optimized thermostatic conditions during expansion and compression, and heat dissipation synchronized at maximum expansion can bring the cycle to be closer to its ideal counterpart, with corresponding improved performance.

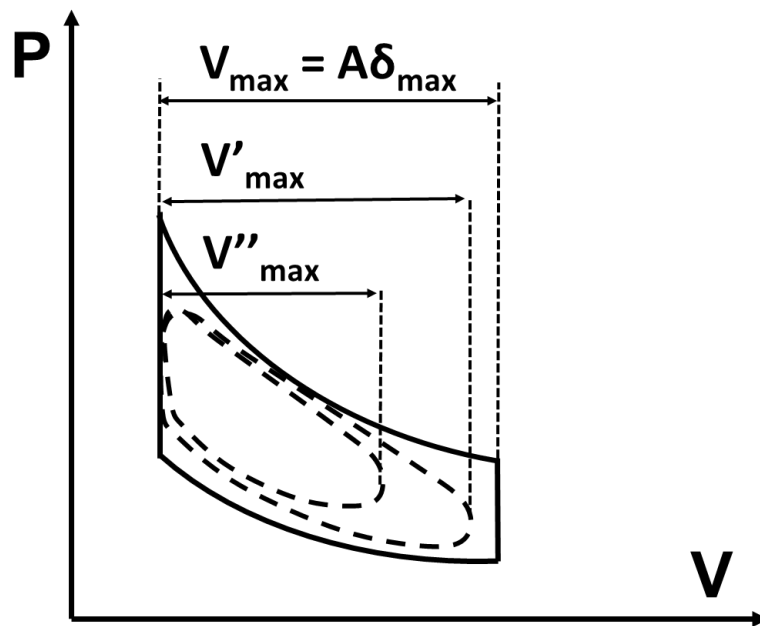


Figure 2. Comparison of ideal and real PV cycles of a photothermal engine. Deviation from the ideal cycle (solid line) is assumed to be mostly from the breakdown of thermostatic conditions during expansion and contraction stages. The resultant cycles (dotted lines) provide reduced expansion ($V''_{max} < V'_{max} < V_{max}$) and reduced deflection of the cantilever ($\delta''_{max} < \delta'_{max} < \delta_{max}$).

Preliminary modeling of an ideal photothermal engine

The fundamental quantities that describe the operation of a photothermal engine based on a solid working medium are the maximum deflection (δ_{max}), the work performed by the medium

to deflect the cantilever (W_{out}), the work performed back on the medium by the returning cantilever (W_{in}), the total work performed on the cantilever over one full cycle ($W_{tot} = W_{out} - W_{in}$), the efficiency (η), and the output power (Π_{out}). Equations 1 to 6 express them as functions of the thermomechanical parameters of the sample and of the difference between the temperature of the two heat reservoirs (T_1 and T_2) of operation (see Supporting Information for derivation). In analogy with the case of a conventional engine, equations 1 – 6 were calculated assuming the case of an AFM tip with a flat contact surface.

$$\delta_{max} = (E_T \alpha_T \Delta T A)/K \quad (1)$$

$$W_{out} = (K \delta_{max}^2)/2 = (E_{T2}^2 \alpha_{T2}^2 \Delta T^2 A^2)/2K \quad (2)$$

$$W_{in} = (K \delta_{max}^2)/2 = (E_{T1}^2 \alpha_{T1}^2 \Delta T^2 A^2)/2K \quad (3)$$

$$W_{tot} = W_{out} - W_{in} = (E_{T2}^2 \alpha_{T2}^2 - E_{T1}^2 \alpha_{T1}^2) \Delta T^2 A^2/2K \quad (4)$$

$$\eta = W_{tot}/Q_{in} = \frac{(E_{T2}^2 \alpha_{T2}^2 - E_{T1}^2 \alpha_{T1}^2) \Delta T^2 A^2}{2 K Q_{in}} \quad (5)$$

$$\Pi_{out} = W_{out}/\Delta\tau_{cycle} \quad (6)$$

E_T : Young's modulus of the material at temperature T . α_T : thermal expansion coefficient of the material at temperature T . $\Delta T (= T_2 - T_1)$: difference between the temperature of the two heat reservoirs. A : area of the tip. K : force constant of the cantilever.

The possibility for this engine to perform extractable total work, W_{tot} , under ideal conditions is dependent on the difference between the thermomechanical properties of the solid working medium at the two temperature extremes. For many common materials, this difference is very small over the temperature difference of operation and total work output is expected to be correspondingly small. Efficiency is also expected to be very small, much smaller than reported for most classical macroscopic engines.

Equations 1 – 6 assume an optimal situation in which the engine is driven by a flat tip, in analogy with the piston of classical engines. This geometry ensures optimal work output and cantilever deflection. However, it is relatively dissimilar from the sample-tip contact realized in a common AFM setup. A common geometry involves a round tip in contact with the sample. This case is better described by using the derivation of the contact area between two compressing spherical bodies, as derived by Hertz. Equations 7 - 11 show the resulting engine performance parameters using Landau's formulation of Hertz's model.⁵ This formalism allows us to describe the more general case of a spherical tip of any material in contact with a curved sample surface.

$$\delta_{max} = E\alpha\Delta T\pi r^2/K \quad (7)$$

$$W_{out} = (E_{T2}^2 \alpha_{T2}^2 \Delta T^2 \pi^2 r^4)/2K \quad (8)$$

$$W_{in} = (E_{T1}^2 \alpha_{T1}^2 \Delta T^2 \pi^2 r^4)/2K \quad (9)$$

$$W_{tot} = (E_{T2}^2 \alpha_{T2}^2 - E_{T1}^2 \alpha_{T1}^2) \Delta T^2 \pi^2 r^4 / 2K \quad (10)$$

$$\eta = \frac{(E_{T2}^2 \alpha_{T2}^2 - E_{T1}^2 \alpha_{T1}^2) \Delta T^2 \pi^2 r^4}{2 K Q_{in}} \quad (11)$$

r is the contact radius of the two spherical bodies and is given by equation 12

$$r^2 = F_{set}^{2/3} D^{2/3} / (1/R + 1/R')^{2/3} \quad (12)$$

F_{set} is the force applied by the tip on the sample, as defined by the AFM setpoint. R and R' are the radii of curvature of the sample and of the tip. In the case of a flat sample, r can be expressed by equation 13.

$$r^2 = (F_{set} D R')^{2/3} \quad (13)$$

The parameter D is a function of Young's modulus for sample and tip (E and E' respectively) and the corresponding Poisson's ratios (σ and σ' respectively).

$$D = \frac{3}{4} ((1-\sigma^2)/E + (1-\sigma'^2)/E') \quad (14)$$

In the case where the modulus of the tip is much larger than the modulus of the sample, equation 14 reduces to equation 15.

$$D = \frac{3}{4} (1-\sigma^2)/E \quad (15)$$

Equation (12) specifically addresses the case of two compressed contacting bodies. Nonetheless the same power dependence between force and contact area is expected for any other geometries.⁵

Experimental Examples

It is useful to provide a real example by using PMMA as the working medium. PMMA is a common material for testing and calibration of AFM-IR experiments and has been systematically used to study the pulse dependence of the experiment. Application of Equations 1 - 15 provides the values in Table I. Table I also includes, for comparison, the efficiency of the ideal Carnot engine, and of the Curzon-Ahlborn engine.

Table I. Photothermal engine parameters calculated for PMMA and specific probe parameters. Data from multiple references.⁶⁻⁸

	Flat Tip Model	Spherical Tip Model (Hertz)	Instrumentation and Experiment Parameters	Sample Parameters (PMMA)
δ_{max}	1.8 nm	2.5×10^{-2} nm	R = 50 nm	$E_{T1} = 3.33 \times 10^9$ GPa
W_{out}	1.6×10^{-18} J	3.1×10^{-22} J	A = 7.8×10^{-15} m ²	$E_{T2} = 3.35 \times 10^9$ GPa
W_{tot}	3.1×10^{-20} J	5.1×10^{-24} J	k = 1 N/m	$\alpha_{T1}^2 = 7.00 \times 10^{-5}$ K ⁻¹
Π_{out}	1.7×10^{-15} W	3.1×10^{-19} W	$\Delta\tau_{cycle} = 1$ ms	$\alpha_{T2}^2 = 7.024 \times 10^{-5}$ K ⁻¹
Π_{tot}	3.1×10^{-17} W	5.1×10^{-21} W	V = A x 100 (nm ³)	$\rho = 1200$ Kg m ⁻³
η	2.2×10^{-5}	2.8×10^{-7}	$F_{set} = 20$ nN	$c_v = 1500$ J K ⁻¹ Kg ⁻¹

η/η_C	0.65%	0.0082 %	$r = 5.8 \text{ nm}$ $\Delta T = 1 \text{ K}$ $T_1 = 295\text{K}$ $T_2 = 296\text{K}$
η/η_{CA}	1.3%	0.016 %	
η_C	3.4×10^{-3}	3.4×10^{-3}	
η_{CA}	1.7×10^{-3}	1.7×10^{-3}	

The projected area of the tip in Table I is the same for both models. However, the sample-tip contact surface is greatly decreased in the case of the spherical tip, resulting in much poorer performance. The maximum deflection, and the expected AFM-IR signal, is two orders of magnitude lower when relying on the spherical tip contact. Work and power output values are four orders of magnitude lower, as expected given the power dependence from the contact area.

Optimizing the performance of an AFM-IR experiment using the photothermal engine model.

Equations 1 - 15 give us guidelines on how to improve the response of the AFM-IR measurement and of the underlying engine.

According to Equation 1, the intensity of the AFM-IR signal parallels the deflection of the cantilever, δ_{\max} . It increases with ΔT and with the optical parameters that affect ΔT , such as the absorption coefficient at the wavelength of excitation. This is the generally accepted dependence of the AFM-IR signal from the macroscopic absorption spectrum of the sample.

The relationship between the AFM-IR signal and the mechanical properties of the sample is also clearly stated by Equation 1. Stiffer materials, with larger values of E , give stronger signal, although this can be curbed by the decrease in α often displayed by the same materials. E is taken to be the Young's modulus of the material, in the assumption that the tip of the cantilever has a very high modulus relative to the sample. If this condition does not hold (e.g. for very stiff samples), the value of E should be the weighed modulus of tip and sample. The signal decreases with increasing K , showing that softer cantilevers provide higher sensitivity. Some of these conclusions have already been inferred from previous theoretical treatments.^{4,8}

The most important point is that equations 1 and 3 also reveal a proportional relationship between the AFM-IR signal and the contact surface between tip and sample. The role of tip-sample contact surface has received little attention in previous theoretical analysis of AFM-IR. Previous theoretical treatments neglect tip shape and tip-sample contact,⁸ or show a dependence from tip radius and do not expand on the implications.⁴ The effect of the tip-sample contact area may be contributing to the difference in signal intensity when measuring convex and concave sample surfaces, together with mechanical factors.⁹ While Equations 1-15 were derived for two specific geometries, the power dependence between contact surface and force is the same for any geometry,⁵ and the proportionality between δ_{\max} and contact area will be retained for any sample and tip structure. Accordingly, it is expected to be a general conclusion that a better match between the shape of the tip and the shape of the sample can extend the contact surface and improve the AFM-IR signal.

A detailed understanding of the nature of heat reservoirs will be relevant for the optimization of AFM-IR measurements in fluids, such as water. To date experiments in an aqueous environment have been analyzed only in terms of mechanical factors, such as the damping of cantilever oscillations in a fluid. A thermodynamic analysis can also guide the design of new instrumental configurations, which depart from the conventional scheme based on cantilever deflection. In a more general sense, the model presented in this work can account for all the

diverse aspects of AFM-IR signal generation, including mechanical, optical, and thermodynamic aspects in one single description.

The quantities that are normally used to characterize the performance of classical engines, i.e. W_{tot} and η , appear to have no direct bearing on the performance of the AFM-IR measurement, in the sense that they do not directly relate to the intensity of the AFM-IR signal. The AFM-IR signal depends on the maximum expansion of the working medium, V_{max} , corresponding to the maximum deflection of the cantilever, δ_{max} . It is not affected by the work needed to compress the sample and by the efficiency of the cycle. Nonetheless, W_{tot} and η do have an influence the AFM-IR experiment. The lower the efficiency, the larger the amount of light energy which is dissipated as heat. In the described engine, even in the absence of plastic deformation of the sample and inelastic processes at the cantilever, most of the energy provided by photons is dissipated as heat. Minimizing heat dissipation through the sample is critical in avoiding sample damage, particularly when handling delicate samples, such as biological samples, with higher intensity of light.

The Photothermal Engine as an Information Producing Mechanism

As already pointed out, the low values of W_{tot} and η are not detrimental factors in the performance of an AFM-IR experiment. This is due to the fundamentally different purpose of the AFM-IR experiment. In contrast to a classical engine, which aims to convert heat into mechanical work, the purpose of the photothermal engine in an AFM-IR experiment is the generation of information. The movement of the engine in response to the presence of an absorbing sample drives the movement of the AFM laser beam on the four-quadrant detector. The movement is read out as a voltage difference, which is proportional to the amplitude of the movement. The voltage reading provides information on the presence or absence of the absorbing material which can be read out as a series of bits, corresponding to a change in information entropy. This will be the subject of a separate analysis.

Pulsed Operation

The cycle described in Figure 1 and Figure 2 implies a quasi-static transformation. In real terms, this condition is not generally realized. Most published experiments involve impulsive excitation, whereby the sample is heated by a laser pulse of brief duration, typically in the nanosecond to microsecond range. Under such conditions, photon absorption produces a rapid increase in pressure and temperature within the sample, leading to its expansion over the time course of a few nanoseconds. The rapid expansion limits the applicability of the quasi-static model of Figure 1. Signal intensity displays a complex dependence from the time structure of pulsed excitation and from the thermal relaxation of the sample between pulses.¹⁰ The expanding sample transfers momentum to the tip and cantilever via a force impulse, triggering its oscillation. In this respect, the response of the cantilever is equivalent to that of a pendulum under the action of an impulsive force normal to its axis. Timing of the impulse with the frequency of the oscillator allows resonant energy transfer processes which greatly enhance the AFM-IR signal.¹¹ A different treatment from the one described in Figure 1 is necessary to fully describe the mechanism involved in pulsed excitation, which accounts for the capability of the oscillating probe to store energy.

Energy transfer to the probe gives rise to an oscillation of the cantilever, the amplitude of which (δ_{max}) is a function of the total work performed on the cantilever, dependent on the duration of

the pulse. Energy transferred from the sample to the cantilever is accumulated as the combination of potential (U) and kinetic (T) energy of the oscillation. In the case of a harmonic oscillator, this is given by equation 16, where m is the mass of the oscillator (approximated by the point mass of the cantilever/tip system positioned at its center of mass), ω_0 its normal frequency, δ_{\max} the amplitude of the oscillation, and K the force constant.

$$U + T = \frac{1}{2} m \omega_0^2 \delta_{\max}^2 = \frac{1}{2} K \delta_{\max}^2 \quad (16)$$

Equation 16 provides the basic indication that increasing the amount of energy transferred to the oscillator, in the absence of dissipative processes, increases the amplitude of the oscillation. In the case of an AFM-IR experiment, a larger oscillation corresponds to an increase in the AFM-IR signal.

In the more general case of a real cantilever, excitation of the oscillation by a single brief impulse leads to simultaneous excitation of multiple modes. The frequency and amplitude of the modes is a function of the geometrical and mechanical properties of the cantilever and of the tip-sample contact. In this respect, resonant mode AFM-IR operation, by which the pulsing frequency of the excitation laser is tuned to match a mechanical resonance of the cantilever, is a specific case of impulsive excitation, leading to the selective amplification of a single mode.

Equation 16 shows that any factors that improve energy transfer to the oscillator in the form of work increase the amplitude of the oscillation and of the resulting AFM-IR signal. Therefore, from a qualitative point of view, the same performance factors can be identified as for the quasi-static process. Considerations about the role of tip sample-contact, of applied setpoint and of thermomechanical properties on the AFM-IR signal, can also be extended to the impulsive process.

Conclusions

The dependence of the AFM-IR signal from heat transfer processes highlights the importance of a thermodynamic analysis of signal generation. In this work we have described the AFM-IR experiment using a quasi-static thermodynamic engine cycle. Based on the engine model we have provided a preliminary theoretical analysis that highlights the main quantities that can affect the performance of the engine and of the associated AFM-IR experiment. We also note that the same parameters can be used as qualitative predictors of performance for the general case of impulsive excitation, although a quantitative treatment for the impulsive case is still missing. We note that, from the perspective of classical thermodynamics, the AFM-IR engine is greatly inefficient. Nonetheless, thermodynamic efficiency, while beneficial, is not the only nor the main performance metric for such system, the main function of which is information production. A notable consequence is that this photothermal engine provides a model system to study the interplay between classical thermodynamics and information theory.

It is important to note that this work describes the AFM-IR experiment using a treatment based on classical thermodynamics and is valid as long as samples can be described by their bulk properties. This is a common regime for AFM-IR samples, which in most cases are thicker than 100 nm. However, AFM-IR experiments also extend to samples 10 nm or less in size, particularly when resonant mode excitation is used. AFM-IR signals can be obtained from samples as thin as a molecular monolayer, and single molecule sensitivity has been reported for larger macromolecules. Such measurements straddle into the realm of single molecule

physics and of quantum mechanics and cannot be satisfactorily described by the macroscopic models provided here.

Acknowledgments

Luca Quaroni was financed by an OPUS16 grant from the National Science Centre Poland under contract 2018/31/B/NZ1/01345.

The author is indebted to Dr Kirk Michaelian, Natural Resources Canada, for discussion in the fundamental aspects of photothermal spectroscopy.

Supporting Information for “Analysis of the Photothermal Engine Cycle in an AFM-IR Measurement of Photothermal Expansion”

Luca Quaroni

Department of Physical Chemistry and Electrochemistry, Faculty of Chemistry, Jagiellonian University, 30-387, Kraków, Poland.

Calculations for an Ideal Photothermal Stirling Engine

Flat piston engine

Maximizing the AFM-IR signal corresponds to maximizing the deflection of the cantilever, δ . The sensitivity of the response is determined by the deflection produced by a unit temperature increase in the sample. In turn, the maximum deflection is determined by balancing the force associated to the expansion of the working medium, F_e , with the force exerted by the cantilever, F_c . F_e is the force exerted by a compressible medium undergoing constrained expansion and is given by Equation s1.

$$F_e = E_T^* \alpha_T \Delta T A \quad (s1)$$

E_T^* is the reduced Young's modulus for the working medium at temperature T . If Young's modulus for the tip is much larger than that for the sample (a common case when using conventional AFM tips of silicon or silicon nitride with soft samples), then E_T^* approximates to E_T for the sample. α_T is the thermal expansion coefficient of the sample at temperature T , ΔT the temperature difference between the two isotherms ($\Delta T = T_2 - T_1$) and A the contact area between tip and sample. This is equivalent to the contact surface of the tip within the assumption that the sample is larger than the tip. Equation 1 assumes a small compression, such that shear stress at the edges of the compression area is negligible.

The deflection of the cantilever, δ , under the action of this force, in the case of harmonic behavior, is given by Hook's Law (Equation s2).

$$F_c = - \delta K \quad (s2)$$

K is the spring constant for the cantilever. The maximum deflection caused by a given temperature increase ΔT is obtained when $F_e = - F_c$ and is given by Equation s3.

$$\delta_{\max} = (E_T \alpha_T \Delta T A)/K \quad (s3)$$

The quantities that describe the performance of an engine are the work associated to this expansion and compression and its overall efficiency. W_{out} is the output work of the engine. This is the work necessary to deflect the cantilever to its maximum extension, δ_{\max} , and is given by Equation s4, where E_{T_2} and α_{T_2} are the values of E and α at the higher temperature T_2 .

$$W_{\text{out}} = (K \delta_{\text{max}}^2)/2 = (E^2_{T_2} \alpha^2_{T_2} \Delta T^2 A^2)/2K \quad (\text{s4})$$

Similarly, the work carried out during the compression stage, W_{in} , is performed after cooling down the medium to the initial temperature T_1 while the cantilever returns to its equilibrium position. It can be obtained using the values of E and α at temperature T_1 (Equation s5).

$$W_{\text{in}} = (K \delta_{\text{max}}^2)/2 = (E^2_{T_1} \alpha^2_{T_1} \Delta T^2 A^2)/2K \quad (\text{s5})$$

As for conventional engines, one useful parameter to describe the performance of the engine is the amount of work produced in a cycle, corresponding to the area of the cycle in the PV diagram. The total work performed by the engine, W_{tot} , is given by Equation s6.

$$W_{\text{tot}} = W_{\text{out}} - W_{\text{in}} = (E^2_{T_2} \alpha^2_{T_2} - E^2_{T_1} \alpha^2_{T_1}) \Delta T^2 A^2 / 2K \quad (\text{s6})$$

As for the case of macroscopic engines, total work increases with the difference between the temperature of the thermal reservoirs used for operation, T_2 and T_1 .

The efficiency of an engine, η , is defined by equation s7.

$$\eta = W_{\text{tot}}/Q_{\text{in}} \quad (\text{s7})$$

Q_{in} is the amount of heat absorbed by the working medium. For our purposes it is useful to equate this to the energy from absorbed light and to express efficiency via Equation s8.

$$\eta = \frac{(E^2_{T_2} \alpha^2_{T_2} - E^2_{T_1} \alpha^2_{T_1}) \Delta T^2 A^2}{2 K Q_{\text{in}}} \quad (\text{s8})$$

The transformations represented in Figure 1 assume quasi static processes, which are infinitely slow. While this condition ensures maximum efficiency, it does not yield any power output. For optimizing performance, we must assess the power output of the system (Π_{out}) under real operating conditions, which can be calculated from the duration of each cycle, $\Delta\tau_{\text{cycle}}$.

$$\Pi_{\text{out}} = W_{\text{out}}/\Delta\tau_{\text{cycle}} \quad (\text{s9})$$

The model described by equations s1-s9 relies on the use of approximations valid for extended samples and for a flat tip-sample contact. These conditions can be met in experiments directed at the characterization of thin films (e.g. to extract thermomechanical as well as spectroscopic parameters of novel materials), or when the interest is in the optimization of micro engine performance.

General Case: two contacting spheres with an external applied force

For applications of the engine to nanoscale spectroscopy, the driving force in AFM-IR development, different models are necessary. The tip-sample interaction force is better described by models that account for the specific geometry of the tip. The force exerted on a spherical tip by the expanding sample, the most common geometry in AFM-IR applications, has already been described.⁵ By using this model we can obtain the relationship between the force applied by the tip (determined by the setpoint) and the mechanical properties of the system and the geometry of the sample. This is given by Equation s10, where R is the radius of the tip and d is the sample thickness.

$$F_e = r^3 (1/R+1/R')/D + E^* \alpha \Delta T \pi r^2 - F_{set} = E^* \alpha \Delta T \pi r^2 \quad (s10)$$

πr^2 is the contact surface between the two compressed spherical bodies. By using Hertz's derivation, as described by Landau⁵, it is shown that r^2 is a function of the mechanical properties of the two spheres and of the applied external force (i.e. the setpoint).

$$r^2 = F_{set}^{2/3} D^{2/3} / (1/R+1/R')^{2/3} \quad (s11)$$

$$r^2 = (F_{set} D R')^{2/3} \quad (s12)$$

$$D = \frac{3}{4} ((1-\sigma^2)/E + (1-\sigma'^2)/E') = \frac{3}{4} (1-\sigma^2)/E \quad (\text{for a hard tip and a soft sample}) \quad (s13)$$

$$\delta_{max} = E \alpha \Delta T \pi r^2 / K \quad (s14)$$

$$W_{out} = (E_{T2}^2 \alpha_{T2}^2 \Delta T^2 \pi^2 r^4) / 2K \quad (s15)$$

$$W_{in} = (E_{T1}^2 \alpha_{T1}^2 \Delta T^2 \pi^2 r^4) / 2K \quad (s16)$$

$$W_{tot} = (E_{T2}^2 \alpha_{T2}^2 - E_{T1}^2 \alpha_{T1}^2) \Delta T^2 \pi^2 r^4 / 2K \quad (s17)$$

$$\eta = \frac{(E_{T2}^2 \alpha_{T2}^2 - E_{T1}^2 \alpha_{T1}^2) \Delta T^2 \pi^2 r^4}{2 K Q_{in}} \quad (s18)$$

References

- 1 L. Quaroni, *Infrared Phys. Technol.*, 2020, **105**, 102779.
- 2 M. S. Anderson, *Appl. Spectrosc.*, 2000, **54**, 349–352.
- 3 A. Dazzi, R. Prazeres, F. Glotin and J. M. Ortega, *Opt. Lett.*, 2005, **30**, 2388–2390.
- 4 A. Dazzi, F. Glotin and R. Carminati, *J. Appl. Phys.*, 2010, **107**, 124519.
- 5 L. D. Landau and E. M. Lifshitz, *Theory Of Elasticity*, Pergamom Press, Oxford, 2nd Editio., 1970.
- 6 V. Shaktawat, N. Jain, N. S. Saxena, K. Sharma and T. P. Sharma, *Polym. Sci. - Ser. B*, 2007, **49**, 236–239.
- 7 R. N. Haward and A. Trainor, *J. Mater. Sci.*, 1974, **9**, 1243–1251.
- 8 A. N. Morozovska, E. A. Eliseev, N. Borodinov, O. S. Ovchinnikova, N. V. Morozovsky and S. V. Kalinin, *Appl. Phys. Lett.*, 2018, **112**, 033105.
- 9 L. Quaroni, *Analyst*, 2020, **145**, 5940–5950.
- 10 L. Quaroni, *Anal. Chem.*, 2020, **92**, 3544–3554.
- 11 F. Lu and M. A. Belkin, *Opt. Express*, 2011, **19**, 19942–7.